

State tomography of capacitively shunted phase qubits with high fidelity

Matthias Steffen, M. Ansmann, R. McDermott, N. Katz, Radoslaw C. Bialczak,

Erik Lucero, Matthew Neeley, E.M. Weig, A.N. Cleland, John M. Martinis*

Department of Physics and California Nanosystems Institute,

University of California, Santa Barbara, CA 93106, USA

(Dated: February 17, 2006)

Abstract

We introduce a new design concept for superconducting quantum bits (qubits) in which we explicitly separate the capacitive element from the Josephson tunnel junction for improved qubit performance. The number of two-level systems (TLS) that couple to the qubit is thereby reduced by an order of magnitude and the measurement fidelity improves to 90%. This improved design enables the first demonstration of quantum state tomography with superconducting qubits using single shot measurements.

PACS numbers:

Superconducting circuits containing Josephson junctions provide a promising approach towards the construction of a scalable solid-state quantum computer [1–6]. The phase qubit [7] has significant potential because coupled qubits have been measured simultaneously [8] and the coherence times are reasonably long [9]. The conventional design of phase qubits relies on the Josephson inductance and the self-capacitance of the Josephson tunnel junction to form a non-linear microwave resonator [7]. Losses and noise in either component compromise qubit performance, however, generally the inductive element has been suspected as the root source of decoherence [10–12]. It therefore came as a surprise when the capacitive element was clearly identified as a main source of decoherence [9]. Because of the large intrinsic loss of the junction capacitor, we believe it is not possible to fabricate high fidelity phase qubits using a standard design and amorphous aluminum oxide (AlO_x) tunnel barriers.

Can we redesign phase qubits to circumvent or minimize capacitive losses without adversely affecting other desirable qubit properties? Understanding this question has profound implications for other designs of superconducting qubits, and may shed light on methods for reducing noise from two-levels systems (TLS).

Here, we introduce a new design concept for superconducting phase qubits with which further progress can be achieved in a straightforward manner. The central idea is to explicitly separate out the capacitive from the inductive element of the Josephson junction, allowing their properties to be separately optimized. This idea can be realized by shunting a tunnel junction, which has little self-capacitance but the same Josephson inductance as the conventional design, with a capacitor which has a lower intrinsic loss tangent than the original junction capacitor, as sketched in Fig. 1(a-c). We have fabricated an improved generation of phase qubits whose measurement fidelity is significantly improved. This success enables the first demonstration of quantum state tomography using a superconducting qubit with single shot measurements.

Progress using phase qubits has thus far been hindered by a large density of TLS defects that couple to the qubit [9]. Individual TLS manifest themselves as avoided level crossings (splittings) in the qubit spectroscopy, as shown in Fig. 2. The defects are located in the insulating barrier of the tunnel junction, and have a significant density because of the relatively large intrinsic loss tangent $\delta_i \sim 1.6 \cdot 10^{-3}$ of AlO_x . Our model predicts that high fidelity phase qubits are not possible using a standard design and amorphous AlO_x tunnel barriers.

However, the number of TLS defects may be dramatically reduced with redesign. Loss of coherence from TLS depends both on the density and size of the splittings, and for low density scales as the square of the tunnel-junction area divided by the total capacitance [9, 13]. A dramatic improvement in fidelity can thus be achieved by reducing the area of the tunnel junction from $\sim 10 \mu\text{m}^2$ to $\sim 1 \mu\text{m}^2$ while holding its critical-current constant, and keeping the total capacitance constant by adding an external low-loss capacitor. With a decrease in the density of splittings, measurement errors [14] are also predicted to lower by a factor of 10. The resulting qubit design of Fig. 1 therefore simply substitutes the lossy capacitance from the tunnel junction with an external element of higher quality. Note that for the standard (single element) design, the junction area scales with the total capacitance and thus loss in coherence scales just as the junction area. The ability to separately control total capacitance and junction area in the new design therefore allows improved protection from decoherence due to individual TLS, in addition to increasing measurement fidelity.

The redesign requires reliable fabrication of tunnel junctions with an area of about $\sim 1 \mu\text{m}^2$. The tunnel barrier is formed by an Ar ion-mill clean followed by thermal oxidation of the Al base electrode. The Josephson junction is next defined by optical lithography and a reactive ion etch in an Ar/Cl plasma. A micrograph of the small-area junction is shown in Fig. 1(b). The shunting capacitor, shown in Fig. 1(c), is made of silicon nitride. It was previously shown to have twenty times lower dielectric loss than SiO_2 [9] and thus is an acceptable choice for this first demonstration.

Experimental tests [14, 15] on the redesigned phase qubit confirm the expected behavior. The number of splittings visible in the qubit spectroscopy is reduced roughly by an order of magnitude, yet their sizes are comparable to those of the conventional design (see Fig. 2). The visibility of the Rabi oscillations (Fig. 3(a)) is about 85% and the decay is limited by the measured energy relaxation time of $T_1 \approx 110$ ns. Because of the small number of splittings, we are able to increase the Rabi oscillation period to about 12.5 ns (limited by pulse shaping and the detuning of ω_{21} [16]), compared to a ~ 50 ns Rabi oscillation period using the conventional design [9].

From the data, we compute a measurement fidelity that is close to 90%. This is an improvement of about 40% compared with the measurement fidelity using the standard phase qubit design. Our observations confirm the prediction that measurement fidelity is reduced by sweeping through avoided level crossings during our measurement pulse [14]. Half of the

remaining 10% loss in the measurement fidelity can be attributed to energy relaxation (as the measurement takes about 5 ns), while the remaining half can be attributed to a loss in signal due to sweeping through a few remaining junction resonances. Additional experimental data, including Ramsey fringes and a Spin Echo (Fig. 3(b) and (c)) are consistent with measured linewidths from the qubit spectroscopy as well as the energy relaxation time.

The energy relaxation of the qubit is limited by the SiN_x shunting capacitor, which has a measured loss tangent of $\delta_i \approx 1.5 \cdot 10^{-4}$. With a qubit frequency $\omega_{10}/2\pi \approx 6$ GHz, we expect an energy relaxation of $T_1 = 1/\delta_i\omega_{10} \approx 170$ ns, which is close to the measured value. Further improvements in T_1 are possible by fabricating shunting capacitors with even lower loss tangents.

The demonstrated improvements in fidelity now enable state tomography, which is necessary for a full characterization of qubit states and gate operations. Typically, state tomography involves measuring an unknown quantum state in different basis sets to extract its location on the Bloch sphere. However, in our experiment it is more convenient to always measure in the $|0\rangle$ and $|1\rangle$ basis, and perform the basis change through single qubit rotations prior to measurement.

To perform tomography, we have designed and built a custom microwave pulse sequencer capable of producing microwave pulses with arbitrary amplitude and phase (see Fig. 4). We use an IQ mixer that adds, with separate amplitude control, the two quadrature components I and Q of a continuous-wave microwave signal. The amplitude of both phases are controlled by an 11-bit digital to analog (DAC) converter that may be updated every 8 ns. A second mixer performs gating and pulse shaping with a time resolution of 1 ns.

We use this microwave pulse sequencer to implement state tomography with two different techniques. The first method simply rotates an unknown Bloch vector over all rotation amplitudes and angles in the $x - y$ plane of the Bloch sphere prior to measuring the final state occupation probability P_1 of $|1\rangle$. From the resulting two-dimensional probability map, the direction of the Bloch vector can be simply computed from the amplitude and phase of the DAC values at maximum P_1 , and the Bloch vector length from the maximum contrast of P_1 .

In Fig. 5 we plot P_1 as a function of amplitude of the I and Q components for several different initial states. In Fig. 5(a) the initial state is the ground state $|0\rangle$, and we observe generalized Rabi oscillations that are independent of the microwave phase, as expected. For

the $|1\rangle$ state of Fig. 5(b), the populations are inverted as compared to (a). In Fig. 5(c) the initial state is the superposition $(|0\rangle + |1\rangle)/\sqrt{2}$, which is pointing along the \hat{x} -direction on the Bloch sphere. As a result, rotations about the \hat{x} -direction (controlled by DAC_Q) will not affect the state. However, rotations along the \hat{y} -direction (controlled by DAC_I) rotate the state and result in Rabi oscillations. The state $(|0\rangle + i|1\rangle)/\sqrt{2}$ is similarly plotted in (d), and shows a 90° rotation in the direction of oscillations as compared to (c). Theoretical predictions are shown in the insets of Fig. 5; small differences arise primarily from off-resonance effects of the $|2\rangle$ state [16].

The data clearly shows this technique can be used to reconstruct an unknown quantum state for *complete* testing of one qubit. However, a more efficient and widely used technique makes use of the fact that any arbitrary single qubit density matrix can be described by $\rho = (I + \sum_{i=1}^3 c_i \sigma_i)/2$ where σ_i denotes the Pauli matrices, I is the identity matrix, and c_i are real coefficients [17, 18]. Therefore, in order to reconstruct an unknown quantum state, we must identify the three-component vector \vec{c} .

The simplest approach measures the three components c_i directly by performing three different read-out schemes. The first read-out is a simple measurement of the state occupation probability of $|1\rangle$, which measures the σ_z component. The second (third) read-out applies a 90° rotation around the \hat{x} -direction (\hat{y} -direction), followed by a measurement of the occupation probability of $|1\rangle$, measuring the σ_y (σ_x) components. Using the three measured occupation probabilities we can reconstruct the quantum state via a least squares fit and place it on the Bloch sphere. Experimentally, this technique is advantageous because it requires only three different read-out sequences instead of acquiring a two-dimensional map.

We use this state tomography to trace out the time evolution of the single qubit quantum state in a Ramsey type experiment, as shown in Fig. 6. In this sequence, we include a current pulse during free evolution to rotate the qubit state about the \hat{z} -axis. This rotation is observed experimentally, and dephasing causes the xy -component to shrink (Fig. 6c, left panel) and relax toward the ground state (Fig. 6c, right panel). These effects are confirmed by a theoretical model which includes energy relaxation and dephasing (see Fig. 6d). The main difference between the experiment and theory is that the length of the reconstructed vector of the first point is about 80% instead of unity. The loss is explained by the 90% measurement fidelity and a time delay of 8 ns between the end of the detuning and the tomography pulses resulting in an additional $\sim 10\%$ loss. The loss due to reduced

measurement fidelities can in principle be compensated by normalizing the data, but this was not done here for clarity.

In conclusion, we have introduced a new design for superconducting phase qubits that explicitly separates the capacitive from the inductive element of the Josephson junction. The number of TLS that couple to the qubit is reduced by an order of magnitude, improving the measurement fidelity to 90% and enabling quantum state tomography. We believe that all aspects of our qubit's performance may now be sufficient to demonstrate violations of Bell's inequalities in coupled qubits. Furthermore, our results pave a clear path towards future improvements in decoherence through the fabrication of simple capacitors with lower dielectric loss.

We acknowledge Steve Waltman and NIST for support in building the microwave electronics. Devices were made at the UCSB and Cornell Nanofabrication Facilities, a part of the NSF funded NNIN network. N. K. acknowledges support of the Rothschild fellowship. This work was supported by ARDA under ARO grant W911NF-04-1-0204 and NSF under grant CCF-0507227.

* Electronic address: `martinis@physics.ucsb.edu`

- [1] Y.A. Pashkin *et al.*, *Nature* **421**, 823 (2003).
- [2] D. Vion *et al.*, *Science* **296**, 886 (2002).
- [3] E. Collin *et al.*, *Phys. Rev. Lett.*, **93**, 157005 (2004)
- [4] I. Chiorescu *et al.*, *Science* **299**, 1869 (2003).
- [5] P. Bertet *et al.*, cond-mat/0412485 [*Phys. Rev. Lett.*, submitted] (2005).
- [6] A. Wallraff *et al.*, *Phys. Rev. Lett.*, **95**, 060501 (2005).
- [7] J.M. Martinis, S. Nam, J. Aumentado, C. Urbina, *Phys. Rev. Lett.*, **89**, 117901 (2002)
- [8] R. McDermott *et al.*, *Science* **307**, 1299 (2005).
- [9] J.M. Martinis *et al.*, *Phys. Rev. Lett.*, **95**, 210503 (2005).
- [10] D.J. Van Harlingen *et al.*, *Phys. Rev. B*, **70**, 064517 (2004)
- [11] F.C. Wellstood, C. Urbina, J. Clarke, *Appl. Phys. Lett.*, **85**, 22, 5296 (2004)
- [12] M. Mück *et al.*, *Appl. Phys. Lett.*, **86**, 012510 (2005)
- [13] Previous work [9] showed that coherence loss scales as N_c^2 , where N_c is the average number of individual TLS that couple to the qubit. The quantity N_c scales as the junction area A_J multiplied by the largest splitting size $S_{\max} \propto 1/\sqrt{C}$, where C is the total capacitance. Loss in coherence thus scales as A_J^2/C .
- [14] K.B. Cooper *et al.*, *Phys. Rev. Lett.*, **93**, 180401 (2004).
- [15] R.W. Simmonds, K.M. Lang, D.A. Hite, S. Nam, D.P. Pappas, J.M. Martinis, *Phys. Rev. Lett.*, **93**, 077003 (2004).
- [16] M. Steffen, J.M. Martinis, I.L. Chuang, *Phys. Rev. B*, **68**, 224518 (2003)
- [17] I.L. Chuang, N. Gershenfeld, M.G. Kubinec, D.W. Leung, *Proc. Roy. Soc. A*, **454**, 447 (1998)
- [18] Y. Liu, L.F. Wei, F. Nori, *Phys. Rev. B*, **72**, 014547 (2005)
- [19] A new design allowed adiabatic changes in the bias current I_J ; to be published.

FIG. 1: Circuit diagram and micrograph of the redesigned phase qubit. (a) A small area ($A_J \sim 1 \mu\text{m}^2$) Josephson junction with little self-capacitance ($C_J = 50 \text{ fF}$) is shunted by a large ($A_C \sim 3600 \mu\text{m}^2$) high quality capacitor with $C_C = 800 \text{ fF}$. The qubit bias current I_J is induced through an inductor with $L = 720 \text{ pH}$. (b) A scanning electron microscope image of the small area Josephson junction shows well defined features at sub-micron length scales. (c) An optical image of the shunting capacitor and the Josephson junction (white circle).

FIG. 2: Qubit frequency $\omega_{10}/2\pi$ versus qubit bias for the conventional single-element design (top trace, shifted for clarity) and the capacitively shunted design (bottom trace). The bias current I_J tunes the frequency of the qubit [14, 15]. The density of splittings in the conventional design is high enough that the qubit is almost always coupled to at least one TLS. The state occupation of $|1\rangle$ is consequently diminished, giving rise to decoherence and thus reducing qubit performance. The new design has about one tenth of the area and consequently exhibits a reduction in the number of avoided level crossings by approximately a factor of ten.

FIG. 3: Experimental results using the capacitively shunted phase qubit design. The vertical axis of each plot displays the probability P_1 of occupying the $|1\rangle$ state. (a) Rabi oscillations have a visibility of about 85% and decay at a rate consistent with the measured qubit relaxation time of $T_1 \approx 110 \text{ ns}$ (shown in (c)). (b) The Ramsey fringes decay non-exponentially and are consistent with spectroscopic linewidths. We extract a dephasing time of $T_2^* \approx 90 \text{ ns}$. (c) The impact of low-frequency $1/f$ noise can be significantly reduced using a Spin Echo sequence. We extract an intrinsic dephasing time of $T_2 \approx 160 \text{ ns}$. Measurement of the energy decay (T_1) is also plotted.

FIG. 4: Schematic diagram of the microwave pulser. The amplitudes of the two quadrature components I and Q are added to obtain microwaves with adjustable amplitude and phase, and are then amplified by 26 dB. A filtered digital pulse is then used in a second mixer to produce a Gaussian-shaped microwave pulse.

FIG. 5: Probability P_1 of occupying state $|1\rangle$ versus DAC_I and DAC_Q , which control the amplitude of the \hat{y} and \hat{x} tomography rotations, for the input states (a) $|0\rangle$, (b) $|1\rangle$, (c) $(|0\rangle + |1\rangle)/\sqrt{2}$, and (d) $(|0\rangle + i|1\rangle)/\sqrt{2}$. The dashed black circle indicates a total pulse amplitude corresponding to a π -pulse at different phases. The white dots label the zero amplitude points, and the three white crosses indicate the measurements necessary for a simplified state tomography technique. The inset in each plot shows the predicted probability map.

FIG. 6: State tomography of the Bloch vector during a Ramsey-type experiment. (a) Sequence of operations of the experiment. A microwave pulse $I_{\mu w}$ at frequency $\omega_{10}/2\pi = 5.838$ GHz is first applied to give a 90° rotation about the \hat{x} -axis. An adiabatic bias pulse I_J [19] is then applied for a time τ_d , during which the qubit is detuned by 37 MHz. The final 90° tomography pulses are 4 ns long, which are short compared with the relaxation times. Each data point was taken with 2,000 statistics and is separated in time by 0.1 ns. (b) Plot of P_1 versus τ_d for the three tomography pulses 90_X , 90_Y , and I . (c) Projections of the reconstructed quantum state on the xy and xz -planes of the Bloch sphere. (d) Theoretical prediction of the evolution of the Bloch vector including relaxation using $T_1 = 110$ ns and $T_2^* = 90$ ns.

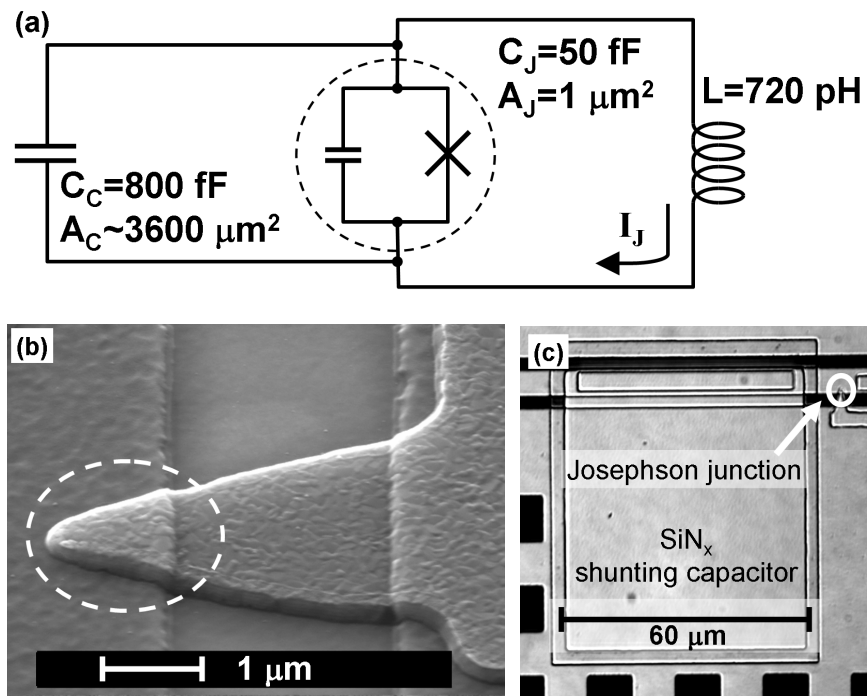


Figure 1

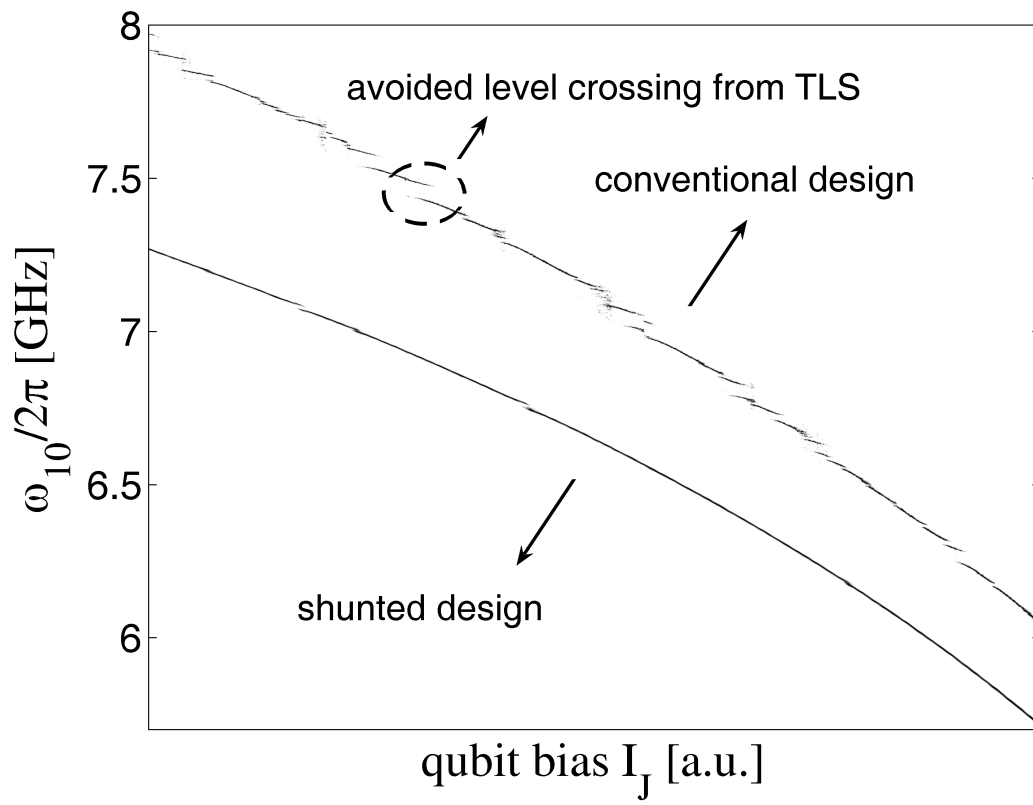


Figure 2

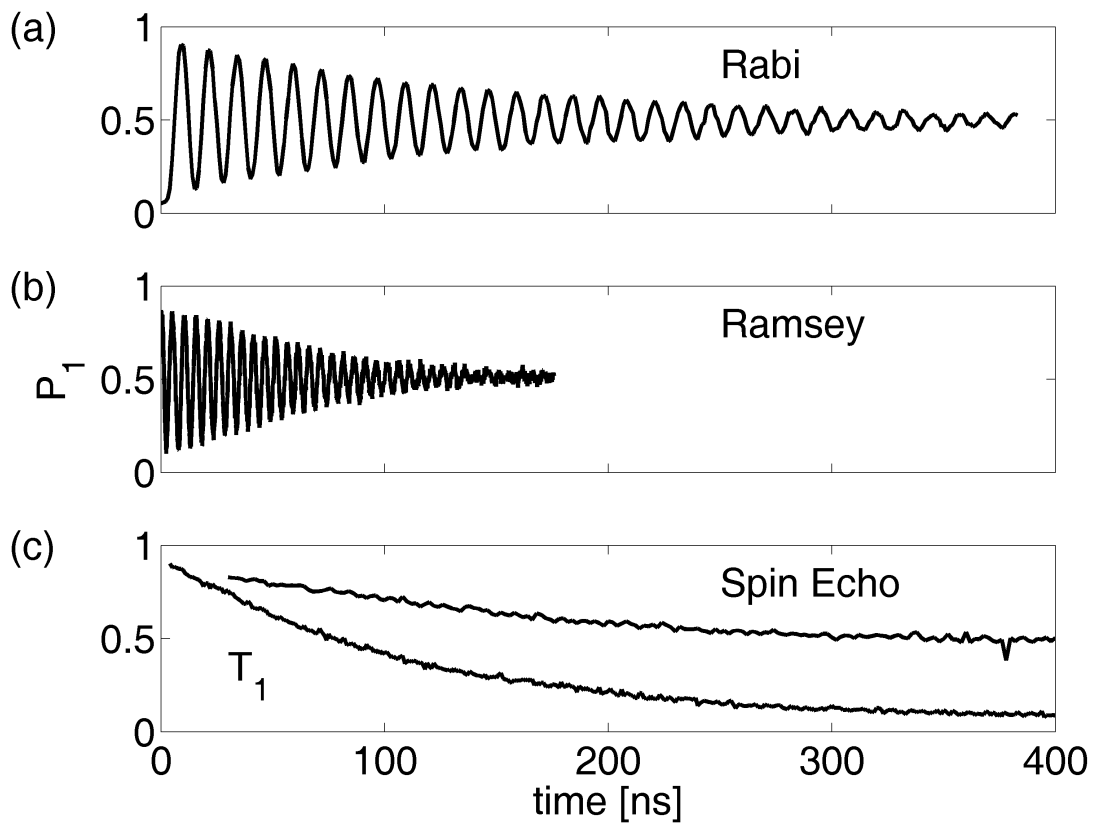


Figure 3

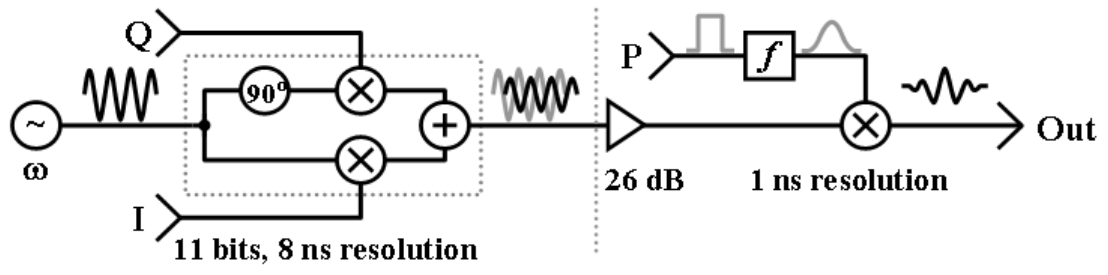


Figure 4

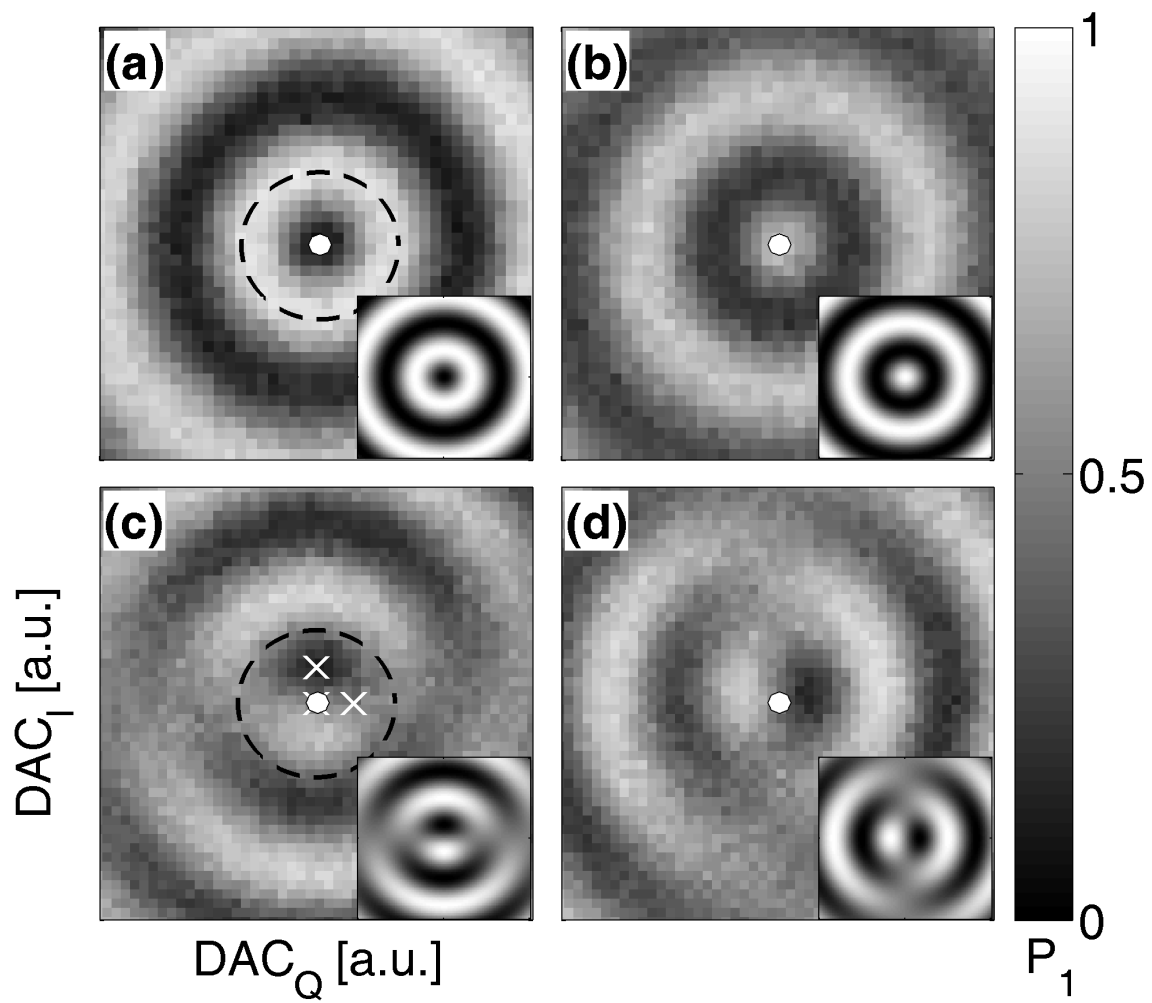


Figure 5

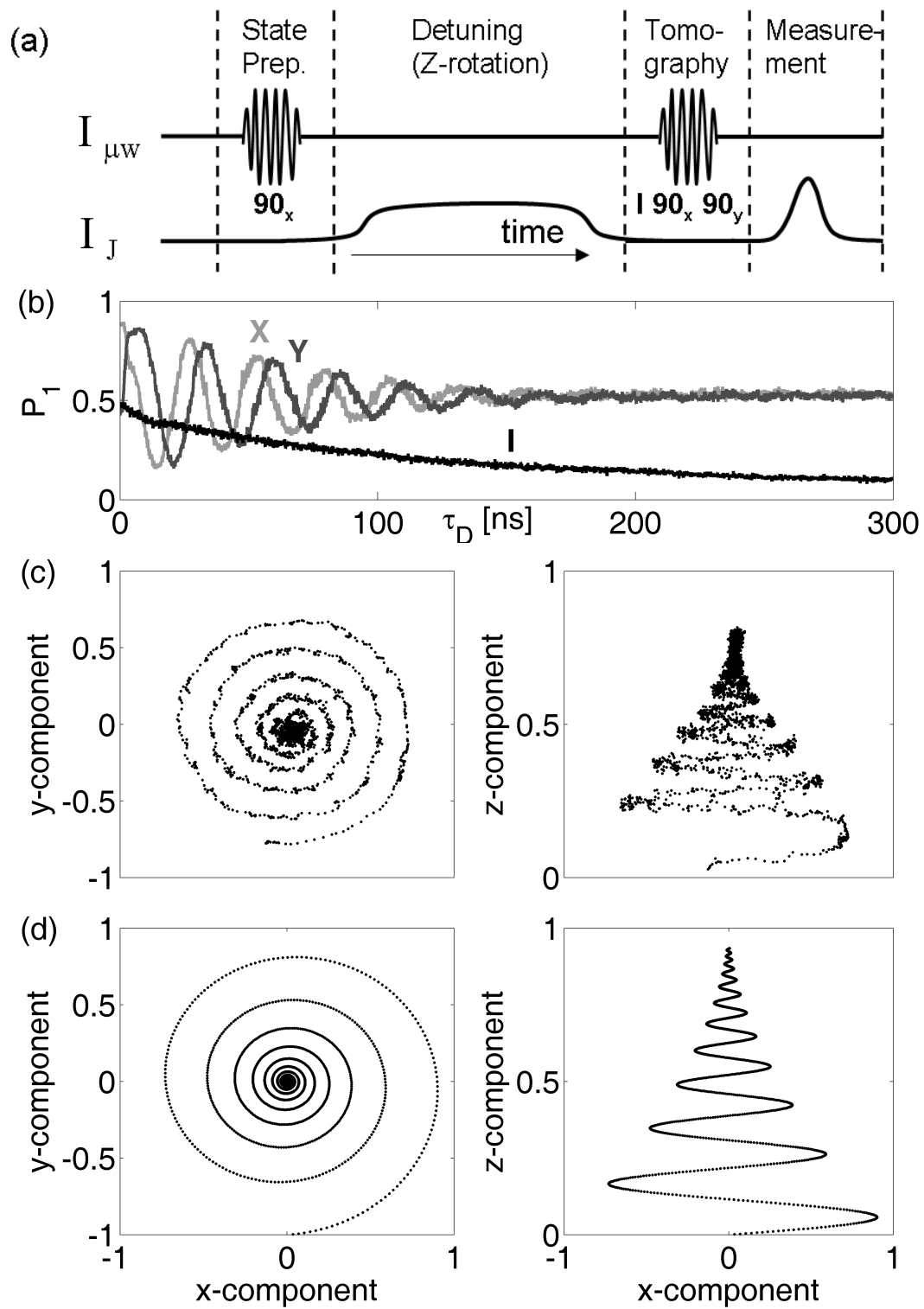


Figure 6